BIOCHEMISTRY
including biophysical chemistry & molecular biology

Article

pubs.acs.org/biochemistry

Role of a Mutated Residue at the Entrance of the Substrate Access Channel in Cytochrome P450 Engineered for Vitamin D_3 Hydroxylation Activity

Hiroaki Fukunishi,*[,†] Hirotaka Yagi,[‡] Ken'ichi Kamijo,[†] and Jiro Shimada[†]

[†]Green Innovation Research Laboratories, NEC Corporation, 34, Miyukigaoka, Tsukuba, Ibaraki 305-8501, Japan

[‡]VALWAY Technology Center, NEC Soft, Ltd., 1-18-7, Shinkiba, Koto-ku, Tokyo 136-8627, Japan

Supporting Information

ABSTRACT: The cytochrome P450 enzyme engineered for enhancement of vitamin D_3 (VD_3) hydroxylation activity, Vdh-K1, includes four mutations (T70R, V156L, E216M, and E384R) compared to the wild-type enzyme. Plausible roles for V156L, E216M, and E384R have been suggested by crystal structure analysis (Protein Data Bank 3A50), but the role of T70R, which is located at the entrance of the substrate access channel, remained unclear. In this study, the role of the T70R mutation was investigated by using computational approaches. Molecular dynamics (MD) simulations and steered molecular dynamics (SMD) simulations were performed, and differences between R70 and T70 were compared in terms of structural change, binding free energy change (PMF), and interaction force between the enzyme and substrate. MD simulations revealed that R70 forms a salt bridge with D42 and the salt bridge affects the locations and the conformations of VD_3 in the bound state. SMD simulations revealed that the salt bridge tends to be formed strongly when VD_3 passes through the binding pocket. PMFs showed that the T70R mutation leads to energetic stabilization of enzyme−VD_3 binding in the region near the heme active site. Interestingly, these results concluded that the D42−R70 salt bridge at the entrance of the substrate access channel affects the region near the heme active site where the hydroxylation of VD_3 occurs; i.e., it is thought that the T70R mutation plays an important role in enhancing VD_3 hydroxylation activity. A significant future challenge is to compare the hydroxylation activities of R70 and T70 directly by a quantum chemical calculation, and three-dimensional coordinates of the enzyme and VD_3 obtained from MD and SMD simulations will be available for the future challenge.

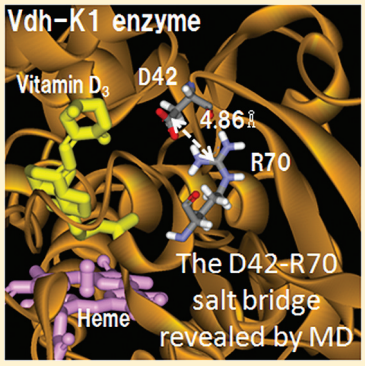

Cytochrome P450 (CYP) enzymes are heme-containing monooxygenases catalyzing diverse reactions in many bacteria and in all archaea, fungi, and higher eukaryotes.[1] In mammals, insects, and plants, they play a critical role in the biosynthesis of sterols, fatty acids, and prostaglandins, and in *Streptomyces* and other bacterial actinomyces, they produce a wide variety of bioactive compounds, including antibacterial, antifungal, antitumor, and immunosuppressive agents.[2] They are also key molecules in human phamacokinetics because they metabolize xenobiotic drugs and toxic chemicals.

Vitamin D_3 (VD_3) is either consumed in food or produced from 7-dehydrocholesterol in the skin upon exposure to sunlight. In humans and other mammals, it has no hormonal activity itself but is a prohormone.[3] Several CYPs convert the substrate into its active form by hydroxylating it. After VD_3 is hydroxylated to 25-hydroxyvitamin D_3 [calcidiol or 25(OH)D_3] by CYP27A1[4,5] and CYP2R1[6] in the liver, the 25(OH)D_3 is hydroxylated to the dihydroxylated metabolite 1α,25(OH)$_2D_3$ by CYP27B1[7] in the kidneys. Only the final product, 1α,25(OH)$_2D_3$, is a hormonally active agent[8−10] mediating biological effects by binding to the vitamin D receptor. Activation of this receptor in the intestine, bone, kidney, and parathyroid gland keeps the calcium and phosphorus concentrations in the blood at the levels needed to maintain bone mineral content.[3,4,11] Indeed, the many symptoms associated with VD_3 deficiency and the VD metabolic disorder, which include psoriasis, osteoporosis, rickets, and hypoparathyroidism, are treated using 1α,25(OH)$_2D_3$ and its derivatives.[3]

Some CYPs in bacteria can hydroxylate VD_3 even though it is not their natural substrate, and the biocatalytic conversion of VD_3 is used in the industrial production of 1α,25(OH)$_2D_3$.[12−14] Fujii et al.[14] recently cloned the gene encoding the VD_3 of actinomycete *Pseudonocardia autotrophica*. This Vdh is a CYP with a sequence that is ∼43% similar with those of members of the CYP107 family and is capable of catalyzing the two-step hydroxylations of VD_3 to 25(OH)VD_3 and then of 25(OH)VD_3 to 1α,25(OH)$_2VD_3$. They furthermore improved the biotransformation of VD_3 to 25(OH)VD_3 by using a combination of random and site-saturated mutagenesis, and they finally obtained the highly active mutant, Vdh-K1. This mutant is a quadruple mutant (T70R/V156L/E216M/E384R) and has

Received: April 28, 2011
Revised: August 30, 2011
Published: August 30, 2011

~21.6 times higher hydroxylase activity than the wild type (Vdh-WT).

Yasutake et al.[15] determined the crystal structures of Vdh-WT in the substrate-free form and Vdh-K1 in the substrate-free, VD_3-bound, and 25(OH)VD_3-bound forms to elucidate the roles of the four mutations. They showed that Vdh-WT exhibits an open conformation with the distal heme pocket exposed to the solvent both in the presence and in the absence of a substrate, whereas Vdh-K1 exhibits a closed conformation in both the substrate-free and substrate-bound forms; they suggested that the four mutations scattered throughout the enzyme shift the conformational equilibrium toward the closed conformation. The substrate-bound structure of Vdh-K1 accommodates both VD_3 and 25(OH)VD_3 but in an antiparallel orientation. The occurrence of the two secosteroid binding modes accounts for the regioselective sequential VD_3 hydroxylations at the C25 and C1α positions of VD_3, i.e., the conversion of VD_3 to 25(OH)VD_3 and then of 25(OH)VD_3 to 1α,25$(OH)_2VD_3$. The crystal structure analysis suggested plausible structural roles for the V156L, E216M, and E384R mutations. In summary, the V156L mutation induces the approximately 8 Å shift of FG helices, the E216M mutation induces conformational changes in the HI loop and extension of helix H, and the E384R mutation increases the stability of the closed conformation; however, the role of the T70R mutation, which is at the entrance of the substrate access channel, remains unclear. Yasutake et al. speculated that R70 of Vdh-K1 may provide a weak primary binding site that improves the efficiency of substrate entry and egress. It has been suggested that arginine residues at the entrance of the substrate access channel in several CYPs also play a crucial role in substrate recognition and/or guiding substrate entry and egress.[16−19] Wade's group investigated the role of arginine (R47) at the entrance of the substrate access channel in cytochrome P450BM-3 by random expulsion dynamics (REMD) simulations.[17,18] Their results suggested that the arginine forms a salt bridge with the negatively charged carboxylic group of the substrate during binding and dissociation. This suggestion is interesting but of questionable relevance to the Vdh-K1 treated in this study because the locations of key arginine residues differ between Vdh-K1 and P450BM-3 and because VD_3 does not include a functional group for forming a salt bridge. Hayashi et al.[19] investigated the roles of two arginines (R73 and R84) in CYP105A1 from *Streptomyces griseolus*, in which R84 is located at the entrance of the substrate access channel. This CYP105A1 is also able to convert VD_3 into its active form, 1α,25$(OH)_2D_3$, by a two-step hydroxylation reaction. The CYP105A1 mutant, which includes R73V and R84A mutations, obtained by site-directed mutagenesis showed much higher activity than the wild type; i.e., the arginines have an inhibitory effect on the enzyme's activity. Their results conflict with that of Fujii et al.,[14] who found that additions of arginine increased the hydroxylation activity.

In this study, we investigated the role of the T70R mutation in the first hydroxylation from VD_3 to 25(OH)VD_3 by using computational approaches, in which molecular dynamics (MD) and steered molecular dynamics (SMD) simulations were performed. SMD simulation, in which an external force is applied to pull a substrate out of a binding site, mimics experimental measurements of pulling a ligand by atomic force microscopy (AFM) but takes place on a different time scale. SMD simulation is effective for investigating structural change and enzyme−substrate interaction thorough the substrate pathway in a binding pocket, and it has been reported that SMD simulations identified the dynamic processes of protein−ligand binding and unbinding.[20−29] From results of MD and SMD simulations, differences between R70 and T70, i.e., between Vdh-K1 and a model enzyme mutated back from R70 to T70, were investigated in terms of the structural change, free energy change (PMF), and interaction force between the enzyme and substrate. In case of nonequilibrium processes such as SMD simulations, PMF can be calculated by using the Jarzynski equality.[30,31] In this way, comparing these characterizations of an individual mutation and its reversion mutant counterpart is helpful for dissecting structure−function relationships.[32]

METHODS

Preparation of Structures. An X-ray crystal structure of the cytochrome P450 mutant (Vdh-K1) in the VD_3-bound form at 2.20 Å resolution [Protein Data Bank (PDB) entry 3A50, chain C][15] was used for preparing initial structures for simulations. Table 1 compares chains A−E in 3A50 in terms of the Cα root-mean-square deviation (rmsd) and distance between D42(CG) and R70(CZ), which is an interaction examined in this study, and Figure S-1 of the Supporting Information shows their chains superposed by an rmsd fit between Cα atoms. Differences between their chains are small enough to be covered by movement of MD simulation even though either chain is selected for MD simulation.

Table 1. Comparison of Five Chains in PDB Entry 3A50

	chain A	chain B	chain C	chain D	chain E
Cα rmsd (Å)[a]	0.00	0.47	0.49	0.56	0.55
D42(CG)−R70(CZ) distance (Å)	9.73	10.47	8.08	8.46	8.99

[a]Chains B−E were superposed on chain A.

Vdh-K1 includes four mutations (T70R, V156L, E216M, and E384R). To compare only the difference between R70 and T70, we built a model structure mutated back from R70 to T70 in Vdh-K1. After the side chain of R70 had been eliminated, the side chain of T70 was generated automatically by the tleap module in Amber version 9.0. Note that this paper refers to Vdh-K1 as K1 and the model enzyme as K1_R70T. For each K1 and K1_R70, 34 Na^+, 12 Cl^-, and 13143 water molecules were added in cubic simulation boxes, and standard protonation states, including neutral His, were assigned for all residues in all proteins by the tleap module. The force fields of parm99[33] and gaff[34] were assigned for the enzyme and for VD_3, respectively. VD_3 was assigned RESP charges as implemented in the resp module of Bayly et al.[35] The crystal structure in the VD_3-bound form has been determined for a ferric state (Fe^{III}) in a high-spin fashion, and the force field developed by Rydberg et al.[36,37] was assigned for porphyrin and some other atoms related to the hydroxylation reaction. Each molecular system for K1 and K1_R70T was minimized for 500 steepest-descent steps and 500 conjugate-gradient steps, during which movements of heavy atoms of the enzyme and heme group were restrained with a force constant 2.0 kcal mol^{-1} $Å^{-2}$. After the minimizations, the systems were heated from 0 to 300 K for 20 ps, during which movements of heavy atoms of the enzyme and heme group were restrained. Subsequently, the systems were equilibrated under constant volume (NVT) for 100 ps, during

dx.doi.org/10.1021/bi2006493 | *Biochemistry* 2011, 50, 8302−8310

which movements of main chain atoms of the enzyme were restrained with a force constant 2.0 kcal mol^{-1} Å^{-2}. After that, the systems were equilibrated under constant pressure (NPT) for 100 ps, during which movements of all atoms were allowed. Finally, initial structures of K1 and K1_R70T surrounded by water molecules (salt concentration of 44 mM) were prepared for MD simulations.

Molecular Dynamics (MD) Simulation. For K1 in the substrate-free form, K1 in the VD_3-bound form, and K1_R70T in the VD_3-bound form, 10 ns MD simulations were performed using Amber version 9.0. These simulations were performed under NVT conditions (300 K), which are controlled by Langevin dynamics with a 1 ps^{-1} collision frequency. SHAKE (rigid bonds)[38] was used on all hydrogen-containing bonds. The particle mesh Ewald (PME) method[39,40] with an 8.0 Å cutoff was used for calculating electrostatic interactions.

Steered Molecular Dynamics (SMD) Simulation. In this study, SMD simulation was used to pull a substrate out of a binding site. This situation mimics experimental measurements of pulling a ligand by atomic force microscopy (AFM). Many researchers also have reported that SMD simulations identified the dynamic processes of protein−ligand binding and unbinidng.[20−29] Multiple SMD simulations were performed using Amber version 9.0. In addition to general conditions for MD simulation, conditions for pulling VD_3 were specified for SMD simulation. First, a reaction coordinate was specified as the distance between the iron atom in the heme group and the C3 atom in VD_3 (see the atom numbers in Figure 1). The

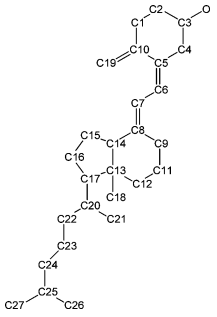

Figure 1. Structure of vitamin D_3 (VD_3).

reaction coordinate is termed heme(Fe)−VD_3(C3). In each SMD simulation, VD_3 was pulled from 20 to 40 Å on the reaction coordinate. The position at 20 Å indicates a stable distance in the VD_3-bound form during 10 ns MD simulations for both K1 and K1_R70T (see Figure S-2 of the Supporting Information), whereas the position at 40 Å indicates a distance completely pulled out of the binding site. Pulling a substrate corresponds to moving the following guiding potential h:

$$h(\mathbf{r};\lambda) = \frac{k}{2}[\xi(\mathbf{r}) - \lambda]^2 \tag{1}$$

where k, $\mathbf{r}$, and $\xi(\mathbf{r})$ are the spring constant, the three-dimensional coordinate, and the position on the reaction coordinate, respectively. An external parameter λ is changed on the reaction coordinate by a constant velocity $v(\lambda_t = \lambda_0 + vt$, where t is time). Note that $\xi(\mathbf{r})$ is constrained near λ by potential h. In this study, the constant pulling velocity was set to 10 Å/ns. The pulling velocity is an important parameter for SMD simulations because higher pulling velocities may lead to significant nonequilibrium effects, which may introduce obvious errors.[41] Several publications have reported the use of pulling velocities in the range of 10−100 Å/ns.[22,24−29,42,43] Therefore, using a value of 10 Å/ns is reasonable. A large spring constant (k = 20000 kcal mol^{-1} Å^{-2}) was used for stiff-spring approximation,[42] which is described in the next section. Under these conditions, a total of 21 SMD simulations were performed from various initial structures at 20 Å on heme(Fe)−VD_3(C3) for K1 and K1_R70T. These initial structures were selected from the 10 ns MD simulation.

Construction of PMF Based on the Jarzynski Equality. The free energy change along a reaction coordinate is termed the potential of mean force (PMF). Generally, the PMF is expressed as a function of coordinate ξ':

$$F(\xi') = -k_B T \ln \int d\mathbf{r}\, d\mathbf{p}\, \delta[\xi(\mathbf{r}) - \xi'] \exp[-\beta H(\mathbf{r},\mathbf{p})] \tag{2}$$

where ξ and H represent a position on the reaction coordinate and a Hamiltonian of the molecular system, respectively, and $\mathbf{r}$ and $\mathbf{p}$ are three dimensional coordinate and momentum, respectively. On the other hand, the PMF based on SMD simulation is expressed by the Hamiltonian of the original system and the guiding potential as a function of external parameter λ correlated to ξ':

$$\begin{aligned}\Phi(\lambda) &= -k_B T \ln \int d\mathbf{r}\, d\mathbf{p} \int d\xi'\, \delta[\xi(\mathbf{r}) - \xi'] \\ &\quad \exp\left\{-\beta H(\mathbf{r},\mathbf{p}) - \beta\frac{k}{2}[\xi(\mathbf{r}) - \lambda]^2\right\} \\ &= -k_B T \ln \int d\xi' \exp\left[-\beta F(\xi') - \beta\frac{k}{2}(\xi' - \lambda)^2\right]\end{aligned} \tag{3}$$

Note that ξ' is constrained near λ. When spring constant k is significantly large, ξ' is approximated by $\xi' \approx \lambda$ (stiff-spring approximation). Consequently, $\Phi(\lambda) \approx F(\lambda)$;[42] i.e., the free energy of the original system can be expressed as a function of external parameter λ.

The Jarzynski equality[30,31] allows us to calculate free energy changes under nonequilibrium processes such as SMD simulations:

$$\exp(-\beta\Delta F) = \langle \exp(-\beta W) \rangle \tag{4}$$

where ΔF and W represent the free energy change and the work of external force in the SMD simulation, respectively, and $\beta = (k_B T)^{-1}$, where k_B and T are the Boltzmann constant and temperature, respectively. The term in broken brackets on the right-hand side is the exponential average, and it is highly possible that insufficient sample data cause large statistical errors. To prevent this problem, the Jarzynski equality is expanded by cumulant expansion as follows:

$$\Delta F = \langle W \rangle - \frac{\beta}{2}(\langle W^2 \rangle - \langle W \rangle^2) + \frac{\beta^2}{6}(\langle W^3 \rangle - 3\langle W^2 \rangle \langle W \rangle + 2\langle W \rangle^3)... \tag{5}$$

and the second-order cumulant is used to suppress statistical error.[42] If the distribution of work W is Gaussian, the third- and

dx.doi.org/10.1021/bi2006493 | Biochemistry 2011, 50, 8302−8310

higher-order cumulants are identically zero and the second-order cumulant is definitely applicable.[42,44] When the second-order cumulant is used, the free energy change is represented as follows:

$$F(\lambda_t) - F(\lambda_0) = \langle W_{0\to t}\rangle - \frac{\beta}{2}(\langle W_{0\to t}^2\rangle - \langle W_{0\to t}\rangle^2) \quad (6)$$

where λ_t and λ_0 represent positions on the reaction coordinate at time t and time zero, respectively. $W_{0\to t}$ represents the work done from time zero to time t.

The statistical reliability was estimated by the standard deviation obtained by using the bootstrap method. This method is generally used for estimating population properties by measuring the empirical distribution of the observed data. The empirical distribution is measured from a number of data sets resampled by random sampling with replacements from the original observed data set.[45] Here, a set of works obtained from N SMD simulations are represented as follows (N = 21 in this study):

$$W_{\text{set}} = \{W_{0\to t}^1, W_{0\to t}^2, W_{0\to t}^3, ..., W_{0\to t}^N\} \quad (7)$$

The following set A is generated by random sampling with replacement from W_{set}:

$$A = \{W_{0\to t}^{(1)}, W_{0\to t}^{(2)}, W_{0\to t}^{(3)}, ..., W_{0\to t}^{(N)}\} \quad (8)$$

where $W^{(i)} = W^{(j)}$ $(i \neq j)$ is allowed. Repeating the operation M times generates the following sets (M = 300 in this study):

$$B = \{A^{(1)}, A^{(2)}, A^{(3)}, ..., A^{(M)}\} \quad (9)$$

From each data set $A^{(i)}$ in B, the totals of M PMFs are calculated. The average and the standard deviation of their PMFs are regarded as the estimator and the statistical error, respectively.

RESULTS

Structural Analyses by MD Simulations. To confirm equilibration during 10 ns MD simulations, we analyzed trajectories of the Cα rmsd against a crystal structure for both K1 and K1_R70T in the VD_3-bound forms (see Figure S-3 of the Supporting Information). Their fluctuations of Cα rmsd are stable within 1 Å during 10 ns MD simulations. Therefore, these molecular systems are considered to be in thermal equilibrium.

We first paid attention to the mutation site of R70 in the K1 enzyme, in particularl interaction between residues D42 and R70. These residues are far apart on the amino acid sequence and are located at the entrance of the substrate access channel. Figure 2 compares trajectories of distance between D42(CG) and R70(CZ), which is termed D42(CG)−R70(CZ), during 10 ns MD simulations for K1 enzymes in the substrate-free and VD_3-bound forms. When the distance is ∼5 Å, a salt bridge is formed between D42 and R70. Note that the distance in the crystal structure in the VD_3-bound form is 8.08 Å and the D42−R70 salt bridge is not formed. Figure 2a shows that the salt bridge is alternately formed and broken for the substrate-free form, whereas Figure 2b shows that it is formed in most regions for the VD_3-bound form. In the substrate-free form, the distance increases to approximately 13 Å when the salt bridge is broken, whereas in the VD_3-bound form, the distance is less than 8 Å even when the salt bridge is broken. The MD

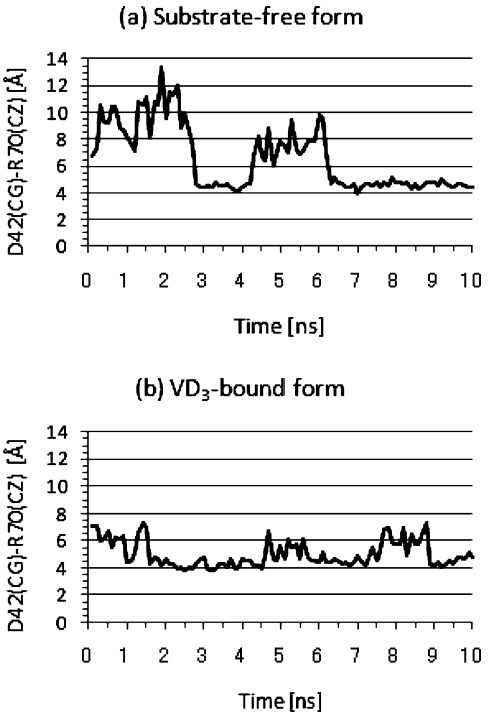

Figure 2. Trajectories of the distance between D42(CG) and R70(CZ), which is termed D42(CG)−R70(CZ), during 10 ns MD simulations for K1 enzymes in the substrate-free and VD_3-bound forms.

structure with the salt bridge is visualized in Figure S-4b of the Supporting Information. These results imply that the D42−R70 salt bridge is important for enhancing VD_3 hydroxylation activity. These results also emphasize the importance of dynamic structural analysis for investigating the role of mutation because the salt bridge could not be confirmed in the crystal structure (PDB entry 3A50). In the results of later SMD simulations, we will discuss the question of whether the D42−R70 salt bridge is formed or broken through the VD_3 pathway in the binding pocket.

Next, we investigated the effect of the D42−R70 salt bridge by comparison of MD structures of K1 and K1_R70T. Naturally, a salt bridge between D42 and T70 in K1_R70T is not formed. Figure 3 shows five MD structures (at 6, 7, 8, 9, and 10 ns) for K1 and K1_R70T, all of which are superposed on the 6 ns MD structure of K1 by an rmsd fit between Cα atoms. Interestingly, the locations and the conformations of VD_3 in the binding pocket clearly differ between K1 and K1_R70T, so the difference is attributed to the D42−R70 salt bridge. VD_3 in K1 moves up to avoid clashing with the salt bridge, whereas VD_3 in K1_R70T moves down in the space between D42 and T70. These results suggest that the VD_3 moving up in the binding pocket is important for VD_3 hydroxylation activity. We also investigated the conformations of the enzymes in the VD_3-bound form depending on whether the salt bridge is formed. Figure 4 compares trajectories of ϕ and ψ angles of R70 of K1 and T70 of K1_R70T during 10 ns MD simulations. The ϕ angle in K1 clearly takes two states of approximately −60° and −120° (the latter angle corresponds to the ends of arrow 2 in Figure S-4c of the Supporting Information). This change in angle is large enough to move the main chain. The ϕ angle in K1_R70T takes one state of approximately −60° in most regions. On the other hand, the ψ

dx.doi.org/10.1021/bi2006493 | Biochemistry 2011, 50, 8302−8310

Figure 3. MD structures at 6, 7, 8, 9, and 10 ns for K1 and K1_R70T enzymes in the VD_3-bound form. Green and orange ribbons represent K1 and K1_R70T enzymes, respectively. All structures are superposed on the 6 ns MD structure of K1 by an rmsd fit between Cα atoms. Blue sticks represent VD_3 and the heme group in K1, and pink sticks represent those in K1_R70T. Colored residues represent D42 and R70 in K1. VD_3 in K1 (blue) moves up to avoid clashing with the salt bridge, whereas VD_3 in K1_R70T (pink) moves down in the space between D42 and T70.

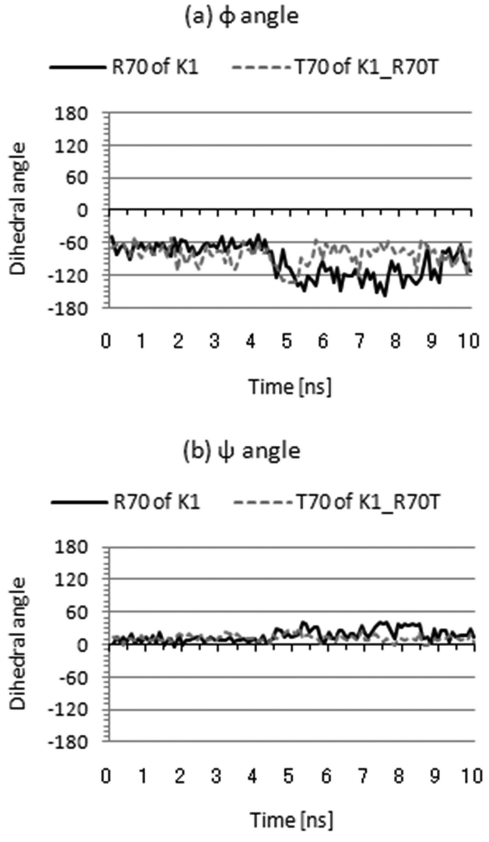

Figure 4. Trajectories of ϕ and ψ angles of R70 of K1 in the VD_3-bound form and T70 of K1_R70T in the VD_3-bound form during 10 ns MD simulations.

angle in K1 takes two states of approximately 10° and 40°, and the former and latter angles correspond to ϕ angles of approximately −60° and −120°, respectively. The ψ angle of K1_R70T takes one state of approximately 10° in most regions. These results suggest that R70 in K1 affects the flexibility of the partial conformation in the region near the entrance of the substrate access channel depending on whether the D42−R70 salt bridge is formed, whereas T70 in K1_R70T tends to strongly maintain the conformation.

Structural Analyses along the VD_3 Pathway in the Binding Pocket by SMD Simulations. In accordance with the results of MD simulations, we paid attention to the D42−R70 salt bridge in K1 enzyme. Figure 5 shows the trajectories of

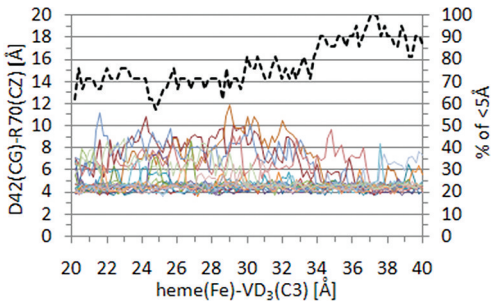

Figure 5. Rate of formation of the D42−R70 salt bridge along the heme(Fe)−VD3(C3) reaction coordinate for K1. The dashed line shows the rate of formation, and solid lines show trajectories of the D42(CG)−R70(CZ) distance for 21 SMD simulations. The salt bridge is formed when the D42(CG)−R70(CZ) distance is <5 Å, and the rate of formation was calculated as a percentage of SMD simulations in which the salt bridge is formed in 21 SMD simulations.

the D42(CG)−R70(CZ) distance during 21 SMD simulations, in which the heme(Fe)−VD_3(C3) reaction coordinate represents the distance between the Fe atom in the heme group and C3 of VD_3. Furthermore, Figure 5 includes the rate of formation of the D42−R70 salt bridge, which is calculated as a percentage of SMD simulations in which the salt bridge is formed in 21 SMD simulations. Formation of the salt bridge is defined as a D42(CG)−R70(CZ) distance of <5 Å. The rate of formation is ∼70% in the range of 20−34 Å and ∼90% in the range of 34−40 Å on the reaction coordinate. This result suggests that the salt bridge is more favorable when VD_3 is located near the entrance of a binding site than when VD_3 is buried deeply in the binding pocket. Here, remember that K1 in the substrate-free form has two states in which the D42−R70 salt bridge is formed or broken, as shown in Figure 2a. Combining the results of Figures 2a and 5 suggests that when K1 recognizes VD_3 near the entrance of the binding site, the salt bridge is likely to be formed.

Next, we investigated the effect of the D42−R70 salt bridge in K1 on the VD_3 pathway in the binding pocket by comparison of 21 SMD structures of K1 and K1_R70T. Figure 6 shows the pathways of VD_3 during 21 SMD simulations, in which all structures for K1 and K1_R70T are superposed on the initial structure of K1 by an rmsd fit between Cα atoms. Representative structures of the enzyme with the heme group for K1 and K1_R70T and 21 VD_3 simulations are shown. The D42−R70 salt bridge in K1 is also shown. When the heme(Fe)−VD_3(C3) distance is 20 Å (Figure 6a), i.e., the initial position in SMD simulation, the conformations of VD_3 between K1 and K1_R70T are clearly different because the salt bridge plays a role in steric hindrance against VD_3 in K1. When the heme(Fe)−VD_3(C3) distance is 25 Å (Figure 6b), they still differ between K1 and K1_R70T. When the heme(Fe)−VD_3(C3) distance is 30 Å (Figure 6c), the VD_3 starts taking

dx.doi.org/10.1021/bi2006493 | Biochemistry 2011, 50, 8302−8310

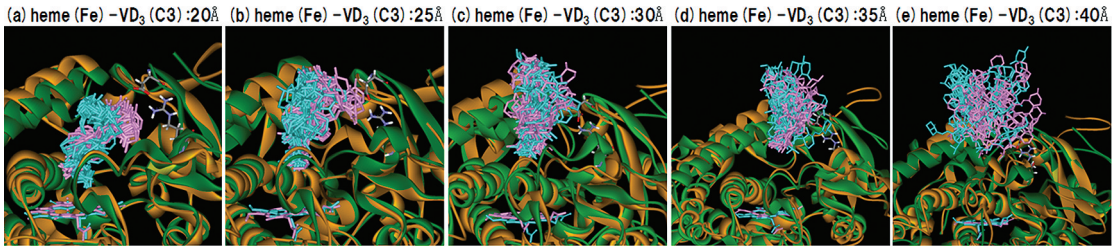

Figure 6. Pathways of VD_3 during 21 SMD simulations. All structures for K1 and K1_R70T enzymes were superposed on the initial structure of K1 by an rmsd fit between Cα atoms. Green and orange solid ribbons represent representative K1 and K1_R70T enzymes, respectively. Blue sticks represent 21 VD_3 simulations and the representative heme group in K1, and pink sticks represent those in K1_R70T. Colored residues represent representative D42 and R70 residues in K1.

various conformations and it becomes difficult to distinguish the conformations of VD_3 between K1 and K1_R70T. When the heme(Fe)−VD_3(C3) distance is 35 Å (Figure 6d), VD_3s are located around the entrance of the binding site and still assemble in an orderly fashion. When the heme(Fe)−VD_3(C3) distance is 40 Å (Figure 6e), they straggle outside the binding site and seem to diffuse freely in solution. From panels d and e of Figure 6, we infer that there is the limit at which K1 and K1_R70T enzymes recognize VD_3 in the range of 35−40 Å.

Energetic and Interaction Force Analyses. As shown in structural analyses, the T70R mutation plays a role in forming the D42−R70 salt bridge and the salt bridge affects the location and conformation of VD_3 in the binding pocket. Here, we investigated effects of the salt bridge in terms of the energetic property and interaction between the enzyme and VD_3. We first investigated the binding free energy change in a reaction coordinate, which is termed the potential of mean force (PMF). In the case of nonequilibrium processes such as SMD simulations, PMF can be calculated by using the Jarzynski equality. It is not easy to obtain a reliable PMF from finite trials of SMD simulations, and we estimated the reliability of PMFs (see Figures S-5 and S-6 of the Supporting Information). As a result, we decided that PMFs in the range of 20−26 Å on the heme(Fe)−VD_3(C3) reaction coordinate are reliable for both K1 and K1_R70T enzymes. PMFs in this range do not correspond to the binding free energy (affinity) between bound and dissociation states, i.e., between 20 and 40 Å. However, PMFs in this range are interesting because this range is especially related to VD_3 hydroxylation activity. Figure 7

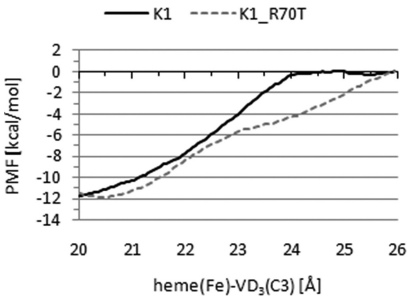

Figure 7. PMFs in the range of 20−26 Å on the heme(Fe)−VD_3(C3) reaction coordinate for K1 and K1_R70T. This region is located near the heme active site where the hydroxylation of VD_3 occurs.

compares PMFs in the range of 20−26 Å between K1 and K1_R70T enzymes for the observation of the energetic effect of the T70R mutation. Note that a zero-point origin of PMFs is at 26 Å. The PMFs of K1 and K1_R70T both change by approximately −12 kcal/mol in the range of 20−26 Å, but their shapes are different. The shape of K1 rapidly changes from 20 to 24 Å and is almost flat from 24 to 26 Å, whereas the shape of K1_R70T changes linearly from 20 to 26 Å. Therefore, the differences in PMF (ΔF) in the range of 20−24 Å are approximately −12 kcal/mol for K1 and approximately −8 kcal/mol for K1_R70T, and K1 and K1_R70T ($\Delta\Delta F$) differ by approximately −4 kcal/mol. This result suggests that K1−VD_3 binding is energetically more stable in the region near the heme active site than K1_R70T−VD_3 binding. It is interesting that the mutation at the entrance of the binding site, which plays a role in forming the D42−R70 salt bridge, affects the binding stability near the heme active site.

Next, we analyzed the mean force corresponding to interaction between the enzyme and VD_3 along the heme-(Fe)−VD_3(C3) reaction coordinate. The mean force is calculated by the differential of PMF: $f_{MF} = -(\Delta F)/(\Delta r)$, where Δr and ΔF represent changes in distance and PMF, respectively (Δr = 0.25 Å in this study). Figure 8 compares

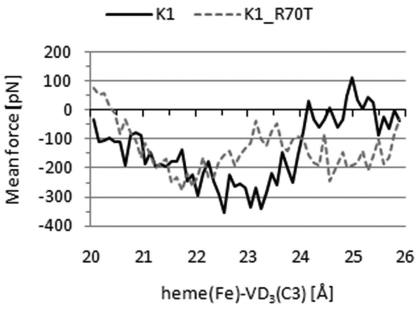

Figure 8. Mean forces in the range of 20−26 Å on the heme(Fe)−VD_3(C3) reaction coordinate for K1 and K1_R70T. This region is located near the heme active site where the hydroxylation of VD_3 occurs.

mean forces in the range of 20−26 Å between K1 and K1_R70T. Negative and positive signs denote inward and outward forces in the binding pocket, respectively. The mean force of K1 is stronger in the ranges of 20−21 and 22−24 Å and weaker in the range of 24−26 Å than that of K1_R70T. Consequently, when VD_3 is located in the region near the heme active site, VD_3 is found to bind to K1 more firmly than to K1_R70T. The range of a mean force depends on that of a PMF because the mean force is calculated by a differential of PMF. On the other hand, an external pulling force calculated directly from the SMD simulation can be obtained throughout the reaction coordinate. The pulling force is calculated by the formula $f_{pull} = -(\Delta W)/(\Delta r)$, where Δr and ΔW represent

dx.doi.org/10.1021/bi2006493 | Biochemistry 2011, 50, 8302−8310

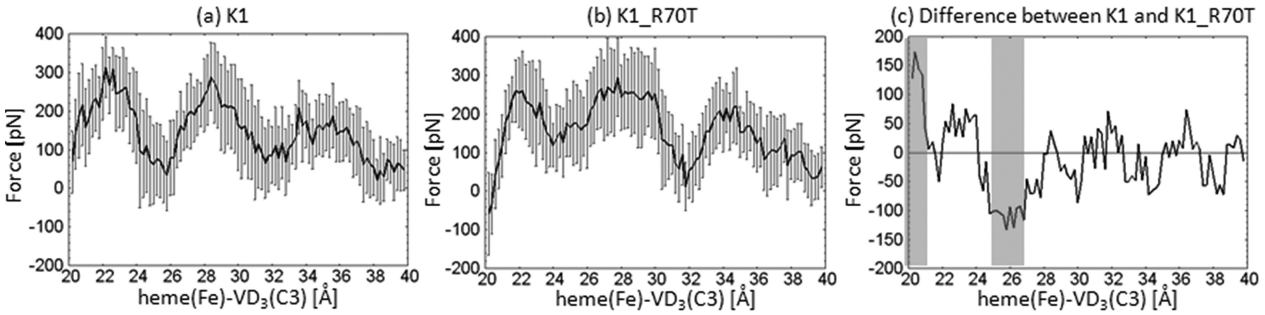

Figure 9. Averages of pulling forces of 21 SMD simulations in the range of 20−40 Å on the heme(Fe)−VD_3(C3) reaction coordinate for (a) K1 and (b) K1_R70T. Error bars represent standard deviations. Panel c shows the difference between K1 and K1_R70T. Transparent boxes represent regions with a large difference (more than ∼100 pN).

changes in the distance and work of pulling VD_3 in SMD simulation, respectively (Δr = 0.25 Å in this study). The pulling force has a tendency similar to that of the mean force, but note that their negative and positive signs are the opposite of those of the mean force. The results of pulling force are useful for roughly estimating the strength of the interaction between the enzyme and VD_3 throughout the reaction coordinate. Figure 9 compares the average of pulling forces of 21 SMD simulations in the range of 20−40 Å on the heme(Fe)−VD_3(C3) reaction coordinate between K1 and K1_R70T. Three peaks of strong pulling force are in the range of 20−40 Å for both K1 and K1_R70T. These peaks are considered to be attributed to favorable interactions or steric hindrance on the pathway of VD_3. Figure 9c shows the difference in average pulling forces between K1 and K1_R70T to clarify the effect of the T70R mutation. There are two regions with a large difference (more than ∼100 pN), and these regions are considered to be strongly affected by the R70T mutation. One is approximately between 20 and 21 Å near the heme active site, and the other is approximately between 24.5 and 27 Å. These results almost correspond to the tendency of the mean forces and support the results of mean forces.

DISCUSSION

Note that this study does not directly estimate chemical reaction associated with the VD_3 hydroxylation activity. The direct estimation of chemical reaction requires a quantum chemical calculation. However, the structural change, binding free energy change, and interaction force between the enzyme and substrate are also important factors for understanding overall enzyme reaction and can be treated in the framework of MD and SMD simulations. So far, the crystal structure analysis by Yasutake et al.[15] suggested structural roles for three of four mutations in Vdh-K1. In summary, the V156L mutation induces the approximately 8 Å shift of FG helices, the E216M mutation induces the conformational change in the HI loop and extension of helix H, and the E384R mutatioon increases the stability of the closed conformation. The last T70R mutation also has structural effects on the formation of the D42−R70 salt bridge and rearrangement of the locations and conformations of VD_3. These structural effects suggest that wild-type CYP enzymes have the potential to catalyze diverse substrates, whereas their three-dimensional structures are not optimized for a specific substrate. That is, mutations leading to structural improvement have the potential to enhance an activity for the specific substrate. Therefore, a primary challenge for the rational design of CYPs is considered to be structural improvement, although a common strategy of rational protein design is improvement of interactions such as electrostatic, van der Waals, and hydrophobic interactions. It is difficult to find mutations inducing structural change in crystal structure analysis, whereas dynamic structural analysis using MD and SMD simulations is a powerful approach for this purpose. For example, introducing a mutation into residue sites with a small fluctuation is considered one approach. Note that this approach does not necessarily enhance enzyme activity but is useful for limiting candidates of the mutation site in a large CYP enzyme.

CONCLUSION

We investigated the role of the T70R mutation at the entrance of the substrate access channel in cytochrome P450 (CYP) engineered for enhancement of VD_3 hydroxylation activity. Molecular dynamics (MD) simulations and steered molecular dynamics (SMD) simulations were performed, and differences between R70 (K1 enzyme) and T70 (K1_R70T enzyme) were compared in terms of structural change, binding free energy change (PMF), and interaction force between the enzyme and substrate. In crystal structure analysis, Yasutake et al.[15] speculated that R70 in the mutant plays a role in guiding substrate entry and egress whereas our study revealed that R70 forms a salt bridge with D42 at the entrance of the substrate access channel. MD simulations revealed that the salt bridge affects the locations and conformations of VD_3 in the bound state. It was shown that VD_3 in K1 moves up to avoid clashing with the salt bridge, whereas VD_3 in K1_R70T moves down in the space between D42 and T70. SMD simulations revealed that the D42−R70 salt bridge tends to be formed strongly when VD_3 passes through the binding pocket and suggested that the salt bridge plays an important role in not only the VD_3-bound state but also the dynamic pathway of VD_3. PMFs showed that the T70R mutation leads to energetic stabilization of enzyme−VD_3 binding in the region near the heme active site where the hydroxylation of VD_3 occurs. Furthermore, mean forces corresponding to interaction between enzyme and VD_3 showed that the T70R mutation leads to strengthening of enzyme−VD_3 in the region near the heme active site. Average pulling forces of SMD simulations also showed equivalent results for the mean forces and supported the mean force results. Interestingly, these structural and energetic results led to the conclusion that the D42−R70 salt bridge at the entrance of the substrate access channel affects the region near the heme active site where the hydroxylation of VD_3 occurs; i.e., it is thought that the T70R mutation plays an important role in enhancing VD_3 hydroxylation activity.

This study demonstrates that dynamic structural analyses by MD and SMD simulations were quite useful in investigating the

dx.doi.org/10.1021/bi2006493 | Biochemistry 2011, 50, 8302−8310

role of mutation because the D42−R70 salt bridge could not be confirmed from the crystal structure (PDB entry 3A50). We therefore consider that this study is one of the most important instances in which molecular simulation complemented crystal structure analysis. A significant future challenge is to compare the hydroxylation activities of R70 and T70 directly by a quantum chemical calculation, and three-dimensional coordinates of the enzyme and VD_3 obtained from MD and SMD simulations will be available for the future challenge.

■ ASSOCIATED CONTENT

Supporting Information

Structural comparison of five chains in PDB entry 3A50, trajectories of the heme(Fe)−VD_3(C3) distance and Cα rmsd during 10 ns MD simulations, structural comparison between crystal and MD structures, and estimation of the reliability of PMFs. This material is available free of charge via the Internet at http://pubs.acs.org.

■ AUTHOR INFORMATION

Corresponding Author

*Phone: +81 29 850 2644. Fax: +81 29 850 6136. E-mail: h-fukunishi@bu.jp.nec.com.

Funding

This work was supported in part by the project on the "Development of Basic Technologies for Advanced Production Methods Using Microorganism Functions" organized by the New Energy and Industrial Technology Development Organization (NEDO).

■ ACKNOWLEDGMENTS

We thank A. Arisawa, Y. Fujii, and members of the Bioresearch Laboratories of Mercian Corp. for providing us with their various biochemical data on P450 Vdh and its mutants prior to publication and for their helpful discussions. We also thank T. Tamura and Y. Yasutake of the Bioproduction Research Institute of AIST for the interpretation of P450 Vdh-K1 structures determined by them and for their helpful discussions. We are grateful to T. Takada (now at MEXT) and members of NEC quantum chemistry group for their kind help.

■ ABBREVIATIONS

MD, molecular dynamics; SMD, steered molecular dynamics; PMF, potential of mean force; K1, VDh-K1; K1_R70T, VDh-K1 form with R70 mutated to T70.

■ REFERENCES

(1) Ortiz de Montellano, P. R. (2005) *Cytochrome P450: Structure, Mechanism, and Biochemistry*, 3rd ed., Kluwer Academic/Plenum Publishers, New York.

(2) Demain, A. L., and Fang, A. (2000) The natural functions of secondary metabolites. *Adv. Biochem. Eng./Biotechnol. 69*, 1−39.

(3) Jones, G., Strugnell, S. A., and DeLuca, H. F. (1998) Current understanding of the molecular actions of vitamin D. *Physiol. Rev. 78*, 1193−1231.

(4) Prosser, D. E., and Jones, G. (2004) Enzymes involved in the activation and inactivation of vitamin D. *Trends Biochem. Sci. 29*, 664−673.

(5) Sawada, N., Sakaki, T., Ohta, M., and Inouye, K. (2000) Metabolism of vitamin D3 by human CYP27A1. *Biochem. Biophys. Res. Commun. 273*, 977−984.

(6) Strushkevich, N., Usanov, S. A., Plotnikov, A. N., Jones, G., and Park, H. W. (2008) Structural analysis of CYP2R1 in complex with vitamin D3. *J. Mol. Biol. 380*, 95−106.

(7) Yamamoto, K., Uchida, E., Urushino, N., Sakaki, T., Kagawa, N., Sawada, N., Kamakura, M., Kato, S., Inouye, K., and Yamada, S. (2005) Identification of the amino acid residue of CYP27B1 responsible for binding of 25-hydroxyvitamin D_3 whose mutation causes vitamin D-dependent rickets type 1. *J. Biol. Chem. 280*, 30511−30516.

(8) Holick, H. L., Schnoes, H. K., and DeLuca, H. F. (1971) 25-Dihydroxycholestecarciferaol, a form of vitamin D_3 metabolically active in the intestines. *Proc. Natl. Acad. Sci. U.S.A. 68*, 803−804.

(9) Lawson, D. E. M., Fraser, D. R. F., Kodicek, E., Morris, H. R., and Williams, D. H. (1971) Identification of 1,25-dihydroxycolestecalciferol, a new kidney hormone controlling calcium metabolism. *Nature 230*, 228−230.

(10) Norman, A. W., Myrtle, J. F., Midgett, R. J., Nowicki, H. G., Williams, V., and Popjak, G. (1971) 1,25-Dihydroxycholestecarciferaol: Identification of the proposed active form of vitamin D_3 in the intestine. *Science 173*, 51−54.

(11) Deeb, K. K., Trump, D. L., and Johnson, C. S. (2007) Vitamin D signaling pathways in cancer: Potential for anticancer therapeutics. *Nat. Rev. Cancer 7*, 684−700.

(12) Sakaki, J., Miyazaki, A., Saito, M., Adachi, T., Mizoue, K., Hanada, K., and Omura, S. (1992) Transformation of vitamin D3 to 1α,25-dihydroxyvitamin D3 via 25-hydroxyvitamin D3 using *Amycolata* sp. strains. *Appl. Microbiol. Biotechnol. 38*, 152−157.

(13) Takeda, K., Asou, T., Matsuda, A., Kimura, K., Okamura, K., Okamoto, R., Sasaki, J., Adachi, T., and Omura, S. (1994) Application of cyclodextrin to microbial transformation of vitamin D3 to 25-hydroxyvitamin D3 and 1α,25-dihydroxyvitamin D3. *J. Ferment. Bioeng. 78*, 380−382.

(14) Fujii, Y., Kabumoto, H., Nishimura, K., Fujii, T., Yanai, S., Takeda, K., Tamura, N., Arisawa, A., and Tamura, T. (2009) Purification, characterization, and directed evolution study of a vitamin D3 hydroxylase from *Pseudonocardia autotrophica*. *Biochem. Biophys. Res. Commun. 385*, 170−175.

(15) Yasutake, Y., Fujii, Y., Nishioka, T., Cheon, W. K., Arisawa, A., and Tamura, T. (2010) Structural evidence for enhancement of sequential vitamin D3 hydroxylation activities by directed evolution of cytochrome P450 Vdh. *J. Biol. Chem. 285*, 31193−31201.

(16) Noble, M., Miles, C., Chapman, S., Lysek, D., MacKay, A., Reid, G., Hanzlik, R., and Munro, A. (1999) Roles of key active-site residues in flavocytochrome P450 BM3. *Biochem. J. 339*, 371−379.

(17) Lüdemann, S. K., Lounnas, V., and Wade, R. C. (2000) Random expulsion molecular dynamics investigation of ligand access channels and mechanisms. *J. Mol. Biol. 303*, 797−811.

(18) Winn, P. J., Lüdemann, S. K., Gauges, R., Lounnas, V., and Wade, R. C. (2002) Comparison of the dynamics of substrate access channels in three cytochrome P450s reveals different opening mechanisms and a novel functional role for a buried arginine. *Proc. Natl. Acad. Sci. U.S.A. 99*, 5361−5366.

(19) Hayashi, K., Sugimoto, H., Shinkyo, R., Yamada, M., Ikeda, S., Ikushiro, S., Kamakura, M., Shiro, Y., and Sakaki, T. (2008) Structure-based design of a highly active vitamin D hydroxylase from *Streptomyces griseolus* CYP105A1. *Biochemistry 47*, 11964−11972.

(20) Izrailev, S., Stepaniants, S., Balsera, M., Oono, Y., and Schulten, K. (1997) Molecular dynamics study of unbinding of the avidin-biotin complex. *Biophys. J. 72*, 1568−1581.

(21) Lüdemann, S. K., Lounnas, V., and Wade, R. C. (2000) How do substrates enter and products exit the buried active site of cytochrome P450cam? 2. Steered molecular dynamics and adiabatic mapping of substrate pathways. *J. Mol. Biol. 303*, 813−830.

(22) Xu, Y., Shen, J., Luo, X., Silman, I., Sussmann, J. L., Chen, K., and Jiang, H. (2003) How does Huperzine A enter and leave the binding gorge of acetylcholinesterase? Steered molecular dynamics simulations. *J. Am. Chem. Soc. 125*, 11340−11349.

(23) Gerini, M. F., Roccatano, D., Baciocchi, E., and Nola, A. D. (2003) Molecular dynamics simulations of lignin peroxidase in solution. *Biophys. J. 84*, 3883−3893.

(24) Bayas, M. V., Schulten, K., and Leckband, D. (2003) Forced Detachment of the CD2-CD58 Complex. *Biophys. J. 84*, 2223−2233.
(25) Zhang, D., Gullingsrud, J., and McCammon, J. A. (2006) Potential of mean force for a acetylcholine unbinding from the α7 nicotinic acetylcholine receptor ligand-binding domain. *J. Am. Chem. Soc. 128*, 3019−3026.
(26) Murcia, M., Faraldo-Gomez, J. D., Maxfield, F. R., and Roux, B. (2006) Modeling the structure of the StART domains of MLN64 and StAR proteins in complex with cholesterol. *J. Lipid Res. 47*, 2614−2630.
(27) Xu, Y., Barrantes, F. J., Shen, J., Luo, X., Zhu, W., Chen, K., and Jiang, H. (2006) Blocking of the Nicotinic Acetylcholine Receptor Ion Channel by Chlorpromazine, a Noncompetitive Inhibitor: A Molecular Dynamics Simulation Study. *J. Phys. Chem. B 110*, 20640−20648.
(28) Zou, H., Zheng, M., Luo, X., Zhu, W., Chen, K., Shen, J., and Jiang, H. (2008) Dynamic Mechanism of Fatty Acid Transport across Cellular Membranes through FadL: Molecular Dynamics Simulations. *J. Phys. Chem. B 112*, 13070−13078.
(29) Murcia, M., Jirouskova, M., Li, J., Coller, B. S., and Filizola, M. (2008) Functional and computational studies of the ligand-associated metal binding site of β3 integrins. *Proteins 71*, 1779−1791.
(30) Jarzynski, C. (1997) Nonequilibrium equality for free energy differences. *Phys. Rev. Lett. 78*, 2690−2693.
(31) Jarzynski, C. (1997) Equilibrium free-energy differences from nonequilibrium measurements: A master-equation approach. *Phys. Rev. E 56*, 5018−5035.
(32) Midelfort, K. S., and Wittrup, K. D. (2006) Context-dependent mutations predominate in an engineered high-affinity single chain antibody fragment. *Protein Sci. 15*, 324−334.
(33) Wang, J. M., Cieplak, P., and Kollman, P. A. (2000) How well does a restrained electrostatic potential (RESP) model perform in calculating conformational energies of organic and biological molecules? *J. Comput. Chem. 21*, 1049−1074.
(34) Wang, J., Wolf, R. M., Caldwell, J. W., Kollamn, P. A., and Case, D. A. (2004) Development and Testing of a General Amber Force Field. *J. Comput. Chem. 25*, 1157−1174.
(35) Bayly, C. I., Cieplak, P., Cornell, W., and Kollman, P. A. (1993) A well-behaved electrostatic potential based method using charge restraints for deriving atomic charges: The RESP model. *J. Phys. Chem. 97*, 10269−10280.
(36) Rydberg, P., Olsen, L., Norrby, P.-O., and Ryde, U. (2007) General transition-state force field for cytochrome P450 hydroxylation. *J. Chem. Theory Comput. 3*, 1765−1773.
(37) Rydberg, P., Hansen, S. M., Kongsted, J., Norrby, P.-O., Olsen, L., and Ryde, U. (2008) Transition-state docking of flunitrazepam and progesterone in cytochrome P450. *J. Chem. Theory Comput. 4*, 673−681.
(38) Ryckaert, J.-P., Ciccotti, G., and Berendsen, H. J. C. (1977) Numerical integration of the Cartesian equations of motion of a system with constraints: Molecular dynamics of n-alkanes. *J. Comput. Phys. 23*, 327−341.
(39) Darden, T., York, D., and Pedersen, L. (1993) Particle Mesh Ewald-an N.Log(N) method for Ewald sums in large systems. *J. Chem. Phys. 98*, 10089−10092.
(40) Essmann, U., Perera, L., Berkowitz, M. L., Darden, T., Lee, H., and Pedersen, L. G. (1995) A smooth particle mesh Ewald potential. *J. Chem. Phys. 103*, 8577−8592.
(41) Isralewitz, B., Gao, M., and Schulten, K. (2001) Steered molecular dynamics and mechanical functions of proteins. *Curr. Opin. Struct. Biol. 11*, 224−230.
(42) Park, S., Khalili-Araghi, F., Tajkhorshid, E., and Schulten, K. (2003) Free energy calculation from nonequilibrium molecular dynamics simulations using Jarzynski's equality. *J. Chem. Phys. 119*, 3559−3566.
(43) Park, S., and Schulten, K. (2004) Calculating potentials of mean force from steered molecular dynamics simulations. *J. Chem. Phys. 120*, 5946−5961.
(44) Hendrix, D. A., and Jarzynski, C. (2001) A "fast growth" method of computing free energy differences. *J. Chem. Phys. 114*, 5974−5981.
(45) Chernick, M. R. (2008) *Bootstrap Methods: A Guide for Practitioners and Researchers*, John Wiley & Sons, New York.